ELSEVIER

Physica B 270 (1999) 118–124

PHYSICA B

# The power absorption and the penetration depth of electromagnetic radiation in lead telluride under cyclotron resonance conditions

S. Özalp[a,*], A. Güngör[b]

[a]*Department of Physics, University of Balıkesir, 10100 Balikesir, Turkey*
[b]*Department of Physics, University of Uludağ, Turkey*

Received 6 April 1998; received in revised form 11 March 1999

**Abstract**

Cyclotron resonance absorption in n- and p-type PbTe was observed by Nii and was analysed under classical skin effect conditions. When the values of DC magnetic field corresponding to peaks are plotted against the field directions, a close fit is obtained between the calculated and observed results based on the assumption of a $\langle 1\,1\,1\rangle$ ellipsoids of revolution model for the both conduction and valance band extrema. From the best fit $m_t = 0.024m_0$ and $0.03m_0$ for the transverse effective masses and $K = m_l/m_t = 9.8$ and 12.2 for the anisotropic mass rations are obtained for the conduction and valance band, respectively. The observed absorption curve shows weak structures at low magnetic field. They are supposed to be due to second harmonics of Azbel'–Kaner cyclotron resonance. However, it turns out to be unnecessary to introduce other bands to explain the experimental results. The applicability of the classical magneto-optical theory is examined by calculating the power absorption coefficient and penetration depth as a function of DC magnetic field.


*Keywords:* IV–VI compounds; PbTe; Penetration depth; Power absorption; Azbel'–Kaner cyclotron resonance; Classical magneto-optical theory

## 1. Introduction

In a paper [1,2] on the experiment of cyclotron resonance absorptions in n- and p-type PbTe, Nii has suggested the following points: (1) the absorption in the region of high magnetic fields is interpreted by classical magneto-optical theory, that is, peaks in this region occur at values of magnetic field corresponding to the dielectric anomaly where the index of refraction vanishes in the dispersion curve: (2) the energy surface of PbTe consists of a set of $\langle 1\,1\,1\rangle$ ellipsoids of revolution for both the conduction and valance band extrema as shown by many other experiments [3–5] and (3) the Azbel'–Kaner cyclotron resonance occurs at low magnetic field.

Prior to Nii's experiment Stiles, Burstein, and Langenberg have observed cyclotron resonance

* Corresponding author. Tel.: + 90-266-249-3358; fax: + 90-266-245-6366.
*E-mail address:* sozalp@zambak.edu.tr (S. Özalp)

0921-4526/99/$ - see front matter 
PII: S0921-4526(99)00167-2

absorption in p-type PbTe [6,7] and concluded that (1) absorption is due to the Azbel's–Kaner cyclotron resonance in the whole range of magnetic field and (2) in addition to the $\langle 1\,1\,1\rangle$ ellipsoids of revolution energy surfaces the valance band has two nearly isotropic energy bands at $k = 0$ whose maxima have the same magnitude as those of the ellipsoids within the error of about $\pm$ 0.002 eV.

It should be especially noted that two peaks which have been attributed to the resonances of heavy and light holes in nearly isotropic bands by Stiles et al. have been also observed by Nii at nearly same values of magnetic field for its given applied direction. Furthermore they are found in both n- and p-type PbTe. This fact is one of the main reasons which have led Nii to propose the explanation above mentioned suggestions. He has interpreted these peaks as being caused by resonances of carriers in the $\langle 1\,1\,1\rangle$ ellipsoidal energy bands.

The aim of this paper is to confirm Nii's suggestion. For this purpose an analysis is performed for classical skin effect conditions based on a set of $\langle 1\,1\,1\rangle$ ellipsoids model for each band. We calculate (i) the angular dependence of the field values corresponding to the absorption peaks in various geometrical configurations and (ii) the line shape of the power the absorption coefficient as a function of magnetic field. Further we examine the applicability of the classical magneto-optical theory by calculating the penetration depth of the electromagnetic field and compare it with the radius of the cyclotron orbit.

In the next section we describe the theoretical procedure to deduce the dispersion relation on the basis of the local treatment of conductivity. In Section 3 the calculated results for directional dependence of field values which correspond to absorption peaks are shown for n- and p-type PbTe. The power absorption curve is calculated in Section 4 in which the collision frequency plays an important role. Finally, in Section 5 it is shown that the penetration depth is always larger than the radius of cyclotron orbit in the range of magnetic fields where strong absorptions are observed.

## 2. The local theory of conductivity and the dispersion relation

The signal detected in the experiment is the energy flow of electromagnetic wave reflected from a sample surface. To obtain it theoretically, it is most important to calculate the complex index of refraction of the electromagnetic wave inside the medium as a function of the static magnetic field. It is given by the Maxwell's equations and the classical equation of motion.

For simplicity we assume that the PbTe sample occupies a semi-infinite space, having a flat surface on which a plane wave is incident normally. Therefore, the electron can move freely along the surface and no depolarisation field occurs in the direction parallel to the surface. In the experiment the surface is always perpendicular to the [0 0 1] direction which we choose as the $x$-axis in a Cartesian coordinate system.

The use of Maxwells equations leads to the expression for the absorption of electromagnetic wave in the Azbel'–Kaner geometry. Thus, the conductivity tensor [8,9] $\boldsymbol{\sigma}$ is obtained as

$$\boldsymbol{\sigma} = \frac{ne^2}{m_0\left(\mathrm{j}\omega + \dfrac{1}{\tau}\right)}(\boldsymbol{m} + \boldsymbol{b}\times\boldsymbol{I})^{-1}, \tag{1}$$

where

$$\boldsymbol{b} = \frac{eH_0}{m_0 c\left(\mathrm{j}\omega + \dfrac{1}{\tau}\right)}$$

and $\boldsymbol{I}$ is the unit tensor. An explicit expression of the inverse tensor $(\boldsymbol{m} + \boldsymbol{b}\times\boldsymbol{I})^{-1}$ in Eq. (1) has been given by Lax et al. [10] When electrons with several kinds of mass exist in the medium, the conductivity tensor is given by

$$\boldsymbol{\sigma} = \sum_i \frac{n_i e^2}{m_0\left(\mathrm{j}\omega + \dfrac{1}{\tau_i}\right)}(\boldsymbol{m}_i + \boldsymbol{b}\times\boldsymbol{I})^{-1}, \tag{2}$$

where the sum is taken over the four valleys which are denoted a, b, c, d.

For our case of n-type PbTe we assume that the conduction band minima consist of four or eight ellipsoids of revolution oriented along the $\langle 1\,1\,1\rangle$

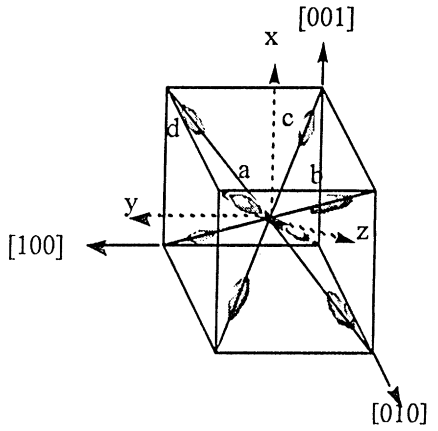


Fig. 1. The conduction band of PbTe consists of a set $\langle 1\,1\,1\rangle$ ellipsoids of revolution a, b, c and d. Long axes are oriented along the $\langle 1\,1\,1\rangle$ directions.

directions in the Brillouin zone and that each valley has the same carrier concentration and the same isotropic relaxation time. We designate the minimum in the [1 1 1], [$\bar{1}$ 1 1] [$\bar{1}$ $\bar{1}$ 1] and [1 $\bar{1}$ 1] directions as valley a, b, c and d, respectively, and choose the [0 0 1], [1 0 0] and [0 1 0] directions as $x$,- $y$,- and $z$-axis (Fig. 1). The mass tensors $\boldsymbol{m}_i$'s in this coordinate system are obtained by the proper unitary transformation from the ellipsoidal mass tensor;

$$\boldsymbol{m} = \begin{pmatrix} m_l & 0 & 0 \\ 0 & m_t & 0 \\ 0 & 0 & m_t \end{pmatrix},$$

where $m_l$ and $m_t$ are the longitudinal and transverse effective masses. For example,

$$\boldsymbol{m} = \begin{pmatrix} m_{||} & m_x & m_x \\ m_x & m_{||} & m_x \\ m_x & m_x & m_{||} \end{pmatrix}$$

where

$$m_{||} = \frac{m_l + 2m_t}{3},$$

$$m_x = \frac{m_l - m_t}{3}.$$

Substituting $m_a \approx m_d$ into Eq. (2) (where $m_d$ and $m_a$ are the effective masses of a and d valleys, respectively) and using the relationship between the complex effective dielectric tensor and the conductivity tensor [8], $\eta_\pm$ is described as a function of applied magnetic field $\boldsymbol{H}_0$. An example of $\boldsymbol{\sigma}$ and $\eta_\pm$ is given in Appendix A when $\boldsymbol{H}_0$ is in a (0 0 1) plane.

In a simple case [7], the power absorption coefficient $A$ is given by

$$A = \frac{4\,\mathrm{Re}\,\eta}{|\eta + 1|^2} \cong \frac{4}{\mathrm{Re}\,\eta} \tag{3}$$

for $|\eta| \geqslant 1$ from the real part of Poynting vector inside the medium. For $\omega\tau \gg 1$, we neglect the term $1/\tau$ in Eq. (2) and $\varepsilon$ becomes an hermitian tensor. Consequently, $\eta^2$ is always real and as easily seen from Eq. (3), an absorption is found for $\eta^2 \geqslant 0$. Namely, it starts at $\eta^2 = \infty$, has a peak as $\eta^2 \to 0$ and is suddenly cut off to zero at $\eta^2 = 0$. This is schematically shown in Fig. 2. Thus the field strength where an absorption peak is observed

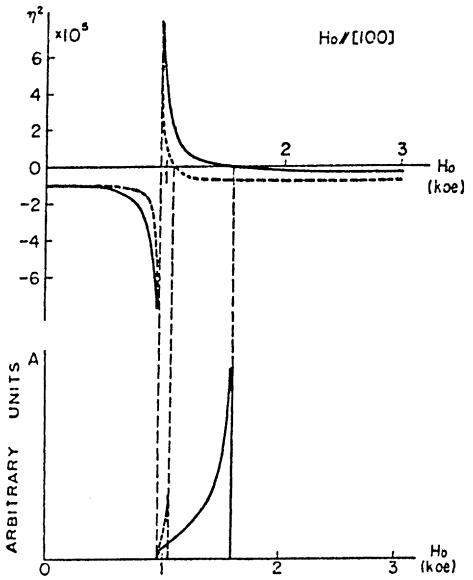


Fig. 2. Plots of the squared index of refraction $\eta^2$ and of the absorption coefficient. $A$ as a function of magnetic field with $\boldsymbol{H}_0 \| [1\,0\,0]$. The calculation is made in the limit of $1/\tau = 0$, using values $m_t = 0.024m_0$ and $m_l = 0.236m_0$ for PbTe. The solid and dashed curves correspond to ordinary and extraordinary modes.

corresponds to the field given theoretically by the condition $\eta^2 = 0$. This condition denotes the dielectric anomaly.

## 3. Comparison of calculated results for n–p-type PbTe with Nii's experimental data

We calculate numerically the field values given by the point $\eta^2 = 0$ as a function of the angle between the field direction and the crystallographic axis. When $H_0$ is in a (0 0 1) plane, for example, we use Eq. (A.5) in Appendix A. The parameters involved are $m_l$ and $m_t$ when $\omega\tau \to \infty$ and $\gamma \to 0$ in Eq. (A.4). They are determined for the conduction electrons as follows:

$$m_l = 0.236,$$

$$m_t = 0.024,$$

$$(K = m_l/m_t = 9.8), \tag{4}$$

by fitting the calculated field strength at points A and B in Fig. 3 to the experimental data. We adjust them more precisely by considering points E, G and I. The calculated values of the points $\eta^2 = 0$ are plotted in a free electron mass unit with bold solid lines. The experimental data for peaks dotted in Fig. 3 fit the calculated curves very closely.

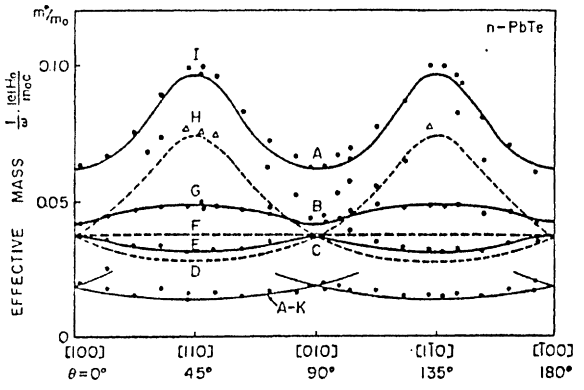


Fig. 3. The values of magnetic field corresponding to the points $\eta^2 = 0$ and $\eta = \infty$ are plotted in free electron mass unit with bold solid and dashed curves against field directions in a (0 0 1) plane. The points are experimental which have been observed for n-PbTe by Nii.

Dashed curves in the figure show the angular variation of the point $\eta^2 = \infty$ which have importance to indicate the field of the onset of an absorption. We have also plotted cyclotron tube mass at which resonance ($\eta^2 = \infty$) does not occur generally.

The dashed curve going through the points D and C indicates a cyclotron tube mass of electrons in valleys a and c which are degenerate for the symmetry of this configuration, and the curve $C$–$H$ is due to electrons in degenerate valleys b and d. The straight line $C$–$F$ shows a value for hybrid resonance which is caused by the interaction of all four valleys The symmetry of the configuration makes it invariant for the change of $\theta$. No absorption peak occurs at point C as schematically shown in Fig. 2. It should be noticed that three solid curves never intersect though dashed curves coincide with each other at the point C. The structures observed at low magnetic fields cannot be expected by the present theory and supposed to be second harmonics of Azbel'–Kaner cyclotron resonance.

Experimental data for p-type sample are also analysed for applied in a (0 0 1) plane. The valance band energy surface is assumed to consist of four or eight ellipsoids of revolution oriented along the $\langle 1\,1\,1 \rangle$ directions. The procedure of calculation and of determination of mass parameters are the same as in mentioned above. The determined effective mass values are

$$m_l = 0.381,$$

$$m_t = 0.031,$$

$$(K = m_l/m_t = 12.2). \tag{5}$$

Numerical result is plotted in Fig. 4 with experimental points.

## 4. Power absorption curve

In this section we calculate the power absorption coefficient by using the effective mass parameters Eq. (4) for n-type PbTe determined in the limit of $\omega\tau \to \infty$ and examine how it fits to the observed absorption curve in which a collision term $\omega\tau$ plays an important role. To obtain it we must solve the problem under the boundary condition for $\boldsymbol{E}, \boldsymbol{H}, \boldsymbol{D}$ and $\boldsymbol{B}$ at the surface of the sample [11–13]. A

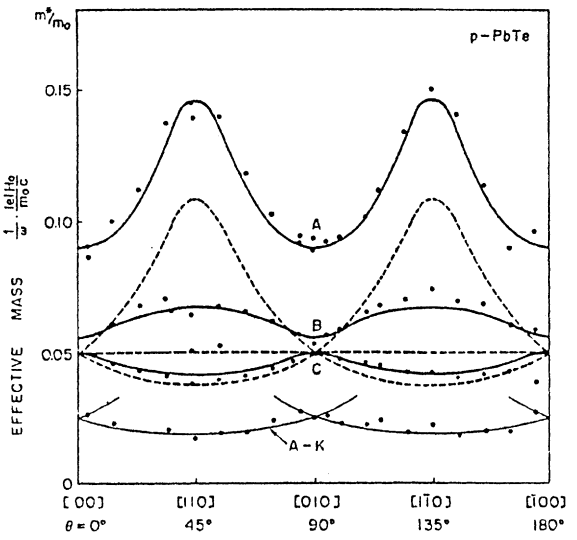


Fig. 4. Plots for PbTe of the points $\eta^2 = 0$ and $\eta^2 = \infty$ vs. field direction in a (0 0 1) plane.

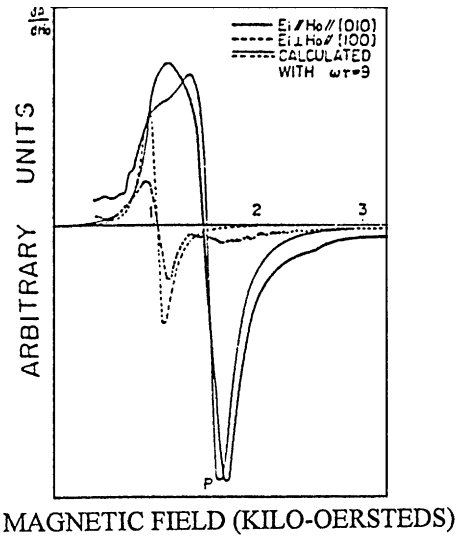


Fig. 5. Calculated and experimental plots of the derivative of power absorption coefficient vs. magnetic field with $\boldsymbol{H}_0 \| [1\,0\,0]$ and $\boldsymbol{H}_0 \| [1\,0\,0]$. The bold lines are observed curves for $\boldsymbol{E}_i \| [0\,1\,0]$ and the light lines are calculated with $\omega\tau = 9$. The solid curves correspond to the ordinary mode ( $\boldsymbol{E}_i \| \boldsymbol{H}_0 \| [0\,1\,0]$) and the dashed to the extraordinary mode ($\boldsymbol{E}_i \perp \boldsymbol{H}_0 \| [1\,0\,0]$). Mass values used in the calculation are $m_t = 0.024 m_0$ and $m_l = 0.236 m_0$.

detailed procedure is omitted here. However, it should be mentioned that the absorption coefficient $A$ is strongly dependent on the direction of incident electric field vector $\boldsymbol{E}_i$, especially the selection rule of absorption is determined by the polarisation of $\boldsymbol{E}_i$. For $\boldsymbol{H}_0$ in a (0 0 1) plane and linearly polarised field $\boldsymbol{E}_i \| [0\,1\,0]$, $A$ is given by

$$A = 1 - R,$$

$$R = \frac{|T(\eta^+ - \eta^-)|^2 + |S(\eta^+ - \eta^-) + \sqrt{S^2 + T^2}.(\eta^+\eta^- - 1)^2|^2}{|(\eta^+ + 1)(\eta^- + 1)\sqrt{S^2 + T^2}|^2} \tag{6}$$

using the notations in Eq. (A.6). $dA/dH_0$ is calculated numerically with $\omega\tau = 9$ as the best-fit value and is plotted in Figs. 5 and 6 as a function of magnetic field. Light and bold curves show calculated and experimental results, respectively. In Fig. 5, the solid curves correspond to the ordinary mode which is allowed $\boldsymbol{E}_i \perp \boldsymbol{H}_0 \| [0\,1\,0]$ and dashed to the extraordinary mode for $\boldsymbol{E}_i \perp \boldsymbol{H}_0 \| [1\,0\,0]$. In Fig. 6 where $\boldsymbol{H}_0 \| [1\,1\,0]$, both modes are admitted since $\boldsymbol{H}_0$ is neither parallel nor perpendicular to $\boldsymbol{E}_i$. A common factor which determines the absolute value of the $dA/dH_0$ curves is obtained by fitting the calculated value to the observed data at the point $P$ in Fig. 5. As seen in Figs. 5 and 6 a fairly good agreement is obtained between the calculated and observed curves, although there remains a little difference in the detailed future. It seems as if the collision time depends on the strength of static magnetic field.

If anomalous skin effect conditions hold, the absorption curves are expected to be almost the same for $\boldsymbol{E} \| \boldsymbol{H}_0$ and $\boldsymbol{E} \perp \boldsymbol{H}_0$.

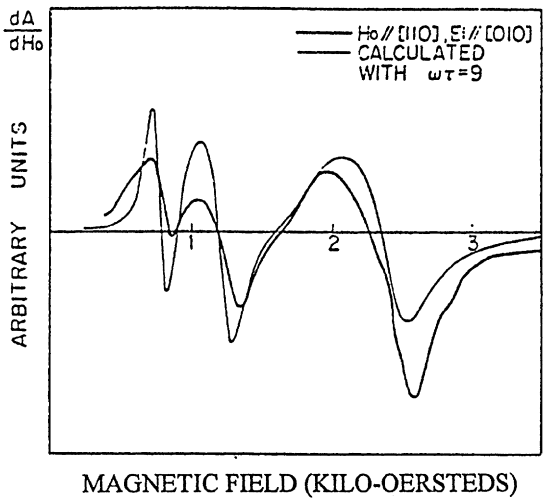


Fig. 6. Calculated and experimental plots of derivative of the power absorption coefficient vs. magnetic field with $\boldsymbol{H}_0\|[1\ 1\ 0]$. Mass values used in the calculation are $m_t = 0.024m_0$ and $m_l = 0.236m_0$. $\boldsymbol{E}_i\|[0\ 1\ 0]$ and $\omega\tau = 9$ are used.

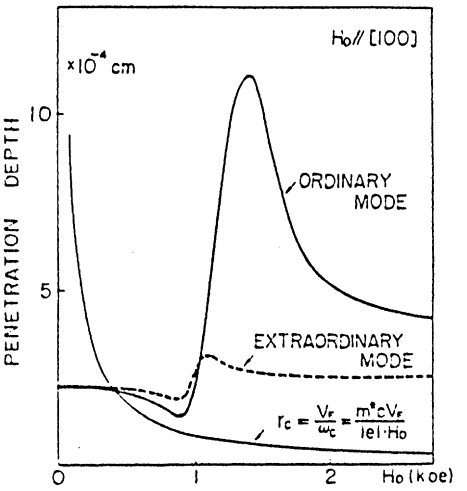


Fig. 7. Plots of the calculated penetration depth and cyclotron radius vs. magnetic field with $\boldsymbol{H}_0\|[1\ 0\ 0]$. Mass values used in the calculation are $m_t = 0.024m_0$ and $m_l = 0.236m_0$ and $\omega\tau = 9$ is used.

## 5. Penetration depth

The penetration depth which is defined by $\xi = -1/\mathrm{Im}\, k$ is plotted in Fig. 7 as a function of magnetic field with $\boldsymbol{H}_0\|[1\ 0\ 0]$. It shows the degree of transmission of the radiation into a sample and is independent of the polarisation of an incident wave. In the figure the bold solid and dashed curves correspond to the ordinary and extraordinary modes, respectively. Thus we can examine whether our treatment under the condition of classical skin effect is correct or not by comparing $\xi$ with a cyclotron orbit radius $r_c = v_F/\omega_c$. The radius $r_c$ is shown by a light solid curve in Fig. 7, where cyclotron frequency $\omega_c = |e|H_0/m^*c$ and Fermi velocity $v_F = 4 \times 10^7$ cm/s are used. We use an appropriate mass value for $m^*$ according to which kinds of electrons are coupling. In the case of Fig. 5 we have used cyclotron tube mass for $m^*$ because cyclotron resonance occurs in this configuration of magnetic field. From Fig. 7 we find that $\xi$ is much larger than $r_c$ at the point where absorption peaks occur.

On the other hand, the situation becomes opposite at the low magnetic field range where weak absorptions are observed in the experiment. Consequently, it is possible that the Azbel'–Kaner cyclotron resonance occurs in this range. Therefore, the result shown in Fig. 7 suggests that our treatment with the classical magneto-optical theory is self-consistent at least in the field where the dielectric anomalies take place.

## 6. Conclusions

Our analysis under the condition of classical skin effect shows an excellent agreement with the experimental results observed by Nii and in fact the calculated penetration depth is much larger than $r_c$ at the high magnetic field where strong absorption occurs. It is clear that the absorption peaks occur at values of magnetic fields corresponding to the dielectric anomalies and that the conduction and valance bands have a set of ellipsoid of revolution energy surfaces oriented along $\langle 1\ 1\ 1 \rangle$ directions. No other band is necessary to explain Nii's experimental data, although the weak structures observed at low magnetic field are attributed to the second harmonics by the Abel'–Kaner cyclotron resonance. Perhaps the isotropic band maxima at

$\boldsymbol{k} = 0$ mentioned by Stiles et al. do not exist within the range of about $\pm$ 0.02 eV (Fermi energy) from those of the ellipsoidal surfaces.

## Appendix A

We calculate the conductivity tensor $\boldsymbol{\sigma}_i$ of each valley by substituting $\boldsymbol{b}$ and $\boldsymbol{m}_i$ into Eq. (2). $\boldsymbol{\sigma}$ is obtained by summing each $\boldsymbol{\sigma}_i$ When $\boldsymbol{\sigma}$ is determined as

$$\boldsymbol{\sigma} = \frac{\sigma_0}{\Delta}\alpha = -\left(\frac{\omega_{p0}}{\omega}\right)^2 \frac{1}{(1-j\upsilon)(\alpha^2-\beta^2)}\alpha, \tag{A.1}$$

$\boldsymbol{\varepsilon}$ is determined as

$$\boldsymbol{\varepsilon} = \varepsilon_l \boldsymbol{I} + \frac{4\pi\sigma_0}{j\omega\Delta}\alpha$$

$$= \left(\frac{\omega_{p0}}{\omega}\right)^2 \left[\gamma \boldsymbol{I} - \frac{1}{(1-j\upsilon)(\alpha^2-\beta^2)}\alpha\right], \tag{A.2}$$

$$\Delta = \alpha^2 - \beta^2,$$

$$\alpha = m_t^2 m_l + m_{||} b^2$$

$$\beta = 2m_x b^2 \sin\theta\cos\theta,$$

$$\alpha_{xx} = (m_{||}^2 - m_x^2)\alpha,$$

$$\alpha_{yy} = (m_{||}^2 - m_x^2 + b^2\cos^2\theta)\alpha$$

$$\alpha_{zz} = (m_{||}^2 - m_x^2 + b^2\sin^2\theta)\alpha,$$

$$\alpha_{xy} = (m_{||}\alpha\sin\theta - m_x\beta\cos\theta)b$$

$$\alpha_{xz} = -(m_{||}\alpha\cos\theta - m_x\beta\sin\theta)b,$$

$$\alpha_{yz} = (m_{||}^2 - m_x^2 + b^2)m_{||}b^2\sin\theta\cos\theta,$$

$$\alpha_{yx} = -\alpha_{xy}, \quad \alpha_{zx} = -\alpha_{xz}, \quad \alpha_{zy} = \alpha_{yz}, \tag{A.3}$$

Where

$$b = \left(\frac{\omega_0}{j\omega}\right)\frac{1}{(1-j\upsilon)}, \quad \omega_0 = \frac{eH_0}{m_0 c}, \quad \upsilon = \frac{1}{\omega\tau},$$

$$\omega_{p0}^2 = \frac{4\pi n e^2}{m_0} \text{ and } \gamma = \varepsilon_l\left(\frac{\omega}{\omega_{p_0}}\right)^2. \tag{A.4}$$

$\theta$ is the angle between the direction of the static magnetic field $H_0$ and [1 0 0] direction. Therefore, the complex index of refraction of the system is obtained as

$$\eta_{\pm}^2 = \left(\frac{\omega_{p0}}{\omega}\right)^2\left[\gamma + \frac{1}{2\alpha_{xx}^*(\alpha^2-\beta^2)(1-j\upsilon)} \times\{-P \pm \sqrt{S^2+T^2}\}\right], \tag{A.5}$$

where

$$\alpha_{xx}^* = \alpha_{xx} - \gamma(1-j\upsilon)(\alpha^2-\beta^2), \quad S = \alpha_{xx}^*(\alpha_{yy}-\alpha_{zz}) + (\alpha_{xy}^2 - \alpha_{xz}^2),$$

$$P = \alpha_{xx}^*(\alpha_{yy}+\alpha_{zz}) + (\alpha_{xy}^2 + \alpha_{xz}^2),$$

$$T = 2(\alpha_{xx}^*\alpha_{yz} + \alpha_{xy}\alpha_{zz}).$$

We have used $\varepsilon_l = 400$ for the lattice dielectric constant of PbTe. $\varepsilon_l(\omega)$ is a tensor, but it can be treated as a scalar in the crystal with cubic symmetry. The lattice dielectric function is given as $\varepsilon_l(\omega) = \varepsilon_\infty(\omega_{L0}^2 - \omega^2 + i\Gamma\omega)/(\omega_{T0}^2 - \omega^2 + i\Gamma\omega)$ and $n = 2\times10^{17}\,\text{cm}^{-3}$ and $\omega = 4.4\times10^{11}\,\text{s}^{-1}$ are given by Nii's experiment.

## References


[1] R. Nii, J. Phys. Soc. Japan 18 (1983) 456.
[2] R. Nii, J. Phys. Soc. Japan 19 (1984) 58.
[3] P.J. Stiles, E. Burstein, D.N. Langenberg, J. Appl. Phys. Suppl. 32 (1981) 2174.
[4] P.J. Stiles, E. Burstein, D.N. Langenberg, Phys. Rev. Lett. 6 (1981) 667.
[5] R.S. Allgaier, J. Appl. Phys. Suppl. 32 (1981) 2185.
[6] P.J. Stiles, E. Burstein, D.N. Langenberg, Phys. Rev. Lett. 9 (1982) 257.
[7] E. Burstein, P.J. Stiles, D.N. Langenberg, R.F. Wallis, Phys. Rev. Lett. 9 (1982) 260.
[8] E.D. Palik, J.K. Furdyna, Rep. Prog. Phys. 33 (1970) 1193.
[9] G. Bauer, in: V.M. Agranovich, A.A. Maradudin (Eds.), Modern Problems in Condensed Matter Sciences, 27, Elsevier Science, North-Holland, 1991, p. 277.
[10] B. Lax, K.J. Button, H.J. Zeiger, M. Roth, Phys. Rev. 102 (1976) 715.
[11] J.K. Galt, W.A. Yager, F.R. Merritt, B.B. Cetlin, A.D. Brailsford, Phys. Rev. 114 (1979) 1396.
[12] G.E. Smith, L.C. Hebel, S.J. Buchsbaum, Phys. Rev. 129 (1983) 154.
[13] S. Yuan, G. Springholz, G. Bauer, Phys. Rev. B 49 (1993) 5479.